Quaternary Science Reviews 300 (2023) 107893

Contents lists available at ScienceDirect

Quaternary Science Reviews

journal homepage: www.elsevier.com/locate/quascirev

Sensitivity of coastal southern African climate to changes in coastline position and associated land extent over the last glacial

Ozan Mert Göktürk [a, b, *], Stefan Pieter Sobolowski [a, c], Margit H. Simon [a, c], Zhongshi Zhang [a, c], Eystein Jansen [a, b]

[a] SFF Centre for Early Sapiens Behaviour (SapienCE), University of Bergen, Post Box 7805, 5020, Bergen, Norway
[b] Department of Earth Science, University of Bergen and the Bjerknes Centre for Climate Research, Bergen, 5007, Norway
[c] NORCE Norwegian Research Centre AS and the Bjerknes Centre for Climate Research, Bergen, 5007, Norway

ARTICLE INFO

Article history:
Received 1 November 2022
Accepted 23 November 2022
Available online 9 December 2022

Handling Editor: C. Hillaire-Marcel

Keywords:
Paleoclimate
Climate
Southern Africa
Modelling
Regional
Local
Sea level
Coastline
Land extent
Marine
Continental
Archaeology

ABSTRACT

Paleoclimatic changes in South Africa, especially around the southern Cape region, are of intense interdisciplinary interest; as this is an important area in the context of human evolution, hosting several prominent archaeological sites such as Blombos Cave (located near today's shoreline). In this study, we investigate the sensitivity of climate of coastal southern Africa to changes in glacial variations in sea level and associated land extent, by performing a model sensitivity experiment. Employing a high-resolution (12 km grid spacing) regional climate model (WRF), output from a global model simulation at 70 thousand years ago (ka) is downscaled twice: First using the present-day coastline, then with an estimated coastline position at 70 ka; keeping all other forcing factors identical. Thus we focus on the response of the local climate to an expanded land surface area equivalent to a glacial sea level low stand scenario. Our results reveal that the climate of previously coastal localities shows strong continental characteristics when sea level drops, as the coastline moves away, and a coastal plain is exposed. This is most evident from the year-round warmer days and cooler nights, with up to 6 °C increases (decreases) in daily maximum (minimum) temperatures. This result also extends to extremes. For instance, at the archaeological site of Blombos Cave, temperature extremes (1st and 99th percentiles) of the modelled marine climate become 25- to 75-fold more probable as the coastline shifts. We also find year-round reductions (5–40%) in the amount of precipitation within the region, owing to local modifications in near-surface atmospheric circulation caused by the exposed land. The reductions in precipitation are accompanied by a significant drop in the annual number of rainy days (31 days locally at Blombos Cave). Simulated changes also vary seasonally, with more pronounced and widespread changes in temperature and precipitation occurring during summer. Through isolating and quantifying the effects of land extent variation, our approach demonstrates, for the first time, the role of coastline position in shaping local climate around near-coastal environs. Our results have significant implications for future studies exploring the influence of local coastline changes on early human settlement and mobility patterns.

1. Introduction

Climate, and its variation across multiple spatial and temporal scales, is recognized as a likely key factor in the survival, migration and evolution of *Homo sapiens* and its extinct relatives (such as Neanderthals) during the last glacial cycle (Eriksson et al., 2012; Timmermann and Friedrich, 2016; Rae et al., 2020; Raia et al., 2020; Timmermann, 2020). However, the robustness of any possible causality relationship between climate and humans is directly dependent on how well past climate is reconstructed. Climate modelling is a powerful tool in this respect, yet, most global models do not provide the level of detail necessary to reflect regional to local scale features. As a result, they miss potentially important information regarding the local environments in which early humans and other hominins lived. For instance, variations in sea level (Lambeck and Chappell, 2001), and associated changes in coastal land extent have potential to significantly affect local-to-regional climate, where early humans often dwelled (Fisher et al.,

* Corresponding author. SFF Centre for Early Sapiens Behaviour (SapienCE), University of Bergen, Post Box 7805, 5020, Bergen, Norway.
E-mail address: ozan.gokturk@uib.no (O.M. Göktürk).

https://doi.org/10.1016/j.quascirev.2022.107893

2020) and travelled through (Lesnek et al., 2018). These influences are important to consider over areas where decreasing/increasing sea levels can result in significant exposure/coverage of coastal plains. Local climatic and ecosystem impacts of such changes in coastal regions have not been studied in detail.

One such region is the southern coast of modern South Africa. The area is highly sensitive to glacial oscillations in sea level, as the Agulhas Bank to its south is known to have been regularly exposed at times of marine regression (Cawthra et al., 2018). For instance, a moderate drop in sea level during a glacial period would significantly shift the coastline, revealing an extensive coastal plain where humans and animals could live and thrive (Fig. 1b). This region also hosts major archaeological sites such as Blombos Cave, Klipdrift Shelter, Klasies River, Diepkloof Rock Shelter and Pinnacle Point 13B (Fig. 1) (Henshilwood et al., 2014; Henshilwood, 2012; Texier et al., 2013; Marean et al., 2007; Wurz, 2002). During interglacials, when sea level was high, people inside Blombos Cave would have looked out at the ocean, from which they collected large amounts of shellfish and other marine resources. During times of decreased sea-level, only a few thousand years later, they would overlook a coastal plain, where herds of grazing animals could be hunted. This exposed landscape, known as the Palaeo-Agulhas Plain (Marean et al., 2020), would have been a rich but entirely different ecosystem, also with a different local climate compared to the rocky coastline of earlier times.

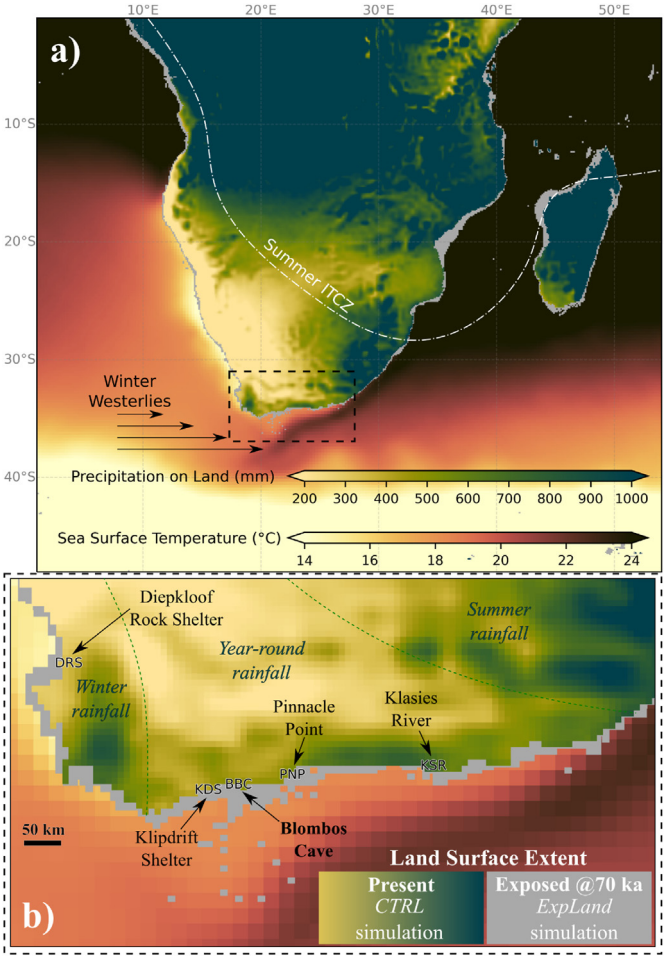

Fig. 1. a) Full domain of the regional climate model utilized in this work (WRF), along with the present day (1991–2020) annual precipitation totals and annually averaged sea surface temperatures (data from ERA5 reanalysis). **b)** Detailed view of the southern Cape region and adjacent areas (dashed rectangle in a)). Exposed land at 70 ka (with respect to present) is shown in grey. Locations of the five archaeological sites cited in the text are also marked. Color maps are after Crameri (2018). (For interpretation of the references to colour in this figure legend, the reader is referred to the Web version of this article.)

Here, we add the broader regional to local climate context to the story and examine the ways in which regional features, namely land-ocean contrasts and highly resolved topography, modulated the impacts of large-scale changes, such as those driven by orbital forcing. To do this we use a regional climate model that has a high level of spatial detail (12 km), focusing on the coastline shifts arising from sea level change. We concentrate on the time around ~70 ka (onset of MIS 4) as this was a period with significant discoveries in Blombos Cave as well as a time when a large area of the coastal plain was exposed. We pay particular attention to changes at Blombos Cave locality as there is ongoing effort for proxy-based climate reconstructions here too, some of which are to be used in follow-up work that will combine data and modelling. Our experimental model set-up in this study allows us to isolate the effects of the coastline shift on local climate at Blombos and other archaeologically important coastal sites in the region. We believe this will allow for a clearer interpretation and contextualization of future results from data-model comparison, and also of archaeological findings from the area.

The rest of the paper is structured as follows. Section 2 provides background concerning present and past climate in the region. Section 3 details the methods and protocols for global and regional climate modelling. Results and discussion are presented in Section 4, followed by summary and conclusions in Section 5.

2. Present and glacial climate in the region

South Africa is situated in an area of the south-north transition from temperate (in southern Cape) to subtropical and tropical zones. Climate models agree that the entire region was cooler during the last glacial, with mean temperatures at the Last Glacial Maximum 2–6 °C lower than the present day (Stone, 2014). Despite the equatorward shift of isotherms in the glacial era, this was still an area of climatic transition, where both midlatitude and tropical weather systems had an influence (Engelbrecht et al., 2019). Accordingly, the amount and seasonality of precipitation have had a large spatiotemporal variation through the late Pleistocene (Simon et al., 2015; Braun et al., 2019) and the Holocene (Strobel et al., 2020). Today, the eastern part of the country, tropically influenced and neighboring the warm Indian Ocean, is remarkably wetter compared to the west (Fig. 1a). Most rainfall in the east falls during austral summer (DJF) due to the regional monsoon circulation, when the ITCZ is at its southernmost position. Long-term variability of summer rainfall is linked to insolation changes, mostly to the orbital precession cycle (Partridge et al., 1997; Simon et al., 2015; Caley et al., 2018).

Today, the amount of precipitation falling in austral winter increases toward the west (Fig. 1b), with moisture arriving mainly from the relatively cooler Atlantic Ocean. It is often carried towards the region by midlatitude depressions, guided by the mean westerly circulation. Still, it is the semi-permanent subtropical high-pressure system over the southern Atlantic that dominates the area. As depressions tend to follow a rather southerly, marine track (Eichler and

Gottschalck, 2013); they quickly weaken or rain out even when they move onshore, usually unable to reach the rain shadows inland. The result is a generally drier western half of the country (compared to the eastern half), where winter precipitation dominates, but is confined to the southwestern and southern Cape regions (Fig. 1b). For instance, the Blombos Cave area receives 56% of its rainfall during the winter half year (Fick and Hijmans, 2017), and the annual total is 500–600 mm; yet these amounts are halved only ~100 km to the north (Cole et al., 2018, Fig. 1b in this paper). Variability of past winter rainfall in the region is less well understood (compared to summer), due to uncertainties regarding the position and strength of southern hemisphere westerlies (Sime et al., 2013).

Coastline shifts and associated changes in land extent over the last glacial period may well have made their own imprint on local climate, modifying key surface variables such as temperature, precipitation, wind direction and speed, which often vary within short distances, especially between coastal areas and their immediate hinterland. It is therefore relevant, in the context of climate influence on humans, to demonstrate how the local climate responded to a retreating shoreline and an expanding coastal plain.

3. Methods

In this study we aimed to isolate the local to regional climate effects of coastline changes. To do this we took a nested modelling approach where a global coupled general circulation model (GCM) was used to generate forcing data for a much higher resolution limited area regional climate model (RCM). Then, using a coastline reconstruction for the period around 70 ka, we performed a time-slice experiment with present and past coastlines. The methods underlying these approaches are detailed in the following subsections.

3.1. Global model protocol

We used the fast version of the Norwegian Earth System Model (NorESM1-F) to conduct the global simulation at 70 ka. NorESM1-F shares many similarities with the Community Climate System Model version 4 (CCSM4), except that the ocean component is replaced with the Miami Isopycnic Coordinate Ocean Model (MICOM). NorESM1-F uses the same atmosphere-land grid as CCSM4, with a horizontal resolution of F19 (~2°) and 26 vertical levels in the atmosphere component. The ocean – sea ice component uses a new tripolar grid with a nominal 1° horizontal resolution. There are 53 vertical layers in the ocean component. Detailed information can be found in Guo et al. (2019). Orbital parameters were taken from Berger and Loutre (1991), greenhouse gas levels from Martínez-Botí et al. (2015), and a global mean sea-level (GMSL) drop of 75 m from (Rohling et al., 2014). We also modify the land-sea distribution arising from the GMSL variations at that time. This GMSL drop makes the Bering Strait closed, and much of the East Siberian continental shelf, Sahul Shelf, and the Sunda Shelf exposed. The experiment was initialized from the Levitus temperature and salinity (Levitus and Boyer, 1994), and then integrated for 3200 years. The model output has a temporal resolution of 6 hours for the atmosphere, 24 hours for land surface, and 1 month for the ocean.

3.2. Regional model protocol

The RCM employed in this study is the Weather Research and Forecasting Model (WRF). WRF is a limited area, non-hydrostatic atmospheric model that is widely used in climate and weather research to obtain spatially detailed information (Powers et al., 2017). In this study, WRF version 4.5.1 (Skamarock et al., 2019) has been set up on a single domain encompassing the entire African continent south of the equator (0° - 50°S, 0° - 55°E; Fig. 1b), at a horizontal resolution of 12 km, and on 35 vertical levels between the surface and ~50 hPa level. The WRF model was used to downscale the output generated by the global NorESM simulation described in the previous subsection and to estimate the sensitivity of regional climate to coastline position. One complete downscaling experiment is a combination of two continuous WRF runs of 10 and 20 years. The forcing data for these two periods were sampled from the NorESM output such that the 30-year temperature and precipitation means of the 20 grid points around southern Africa (Supp. Fig.) are closest to their long-term averages in the entire NorESM output. The aim was to force WRF with climatological boundary conditions obtained over the 160-year NorESM time slice and minimize the influence of internal variability. Such a construction helps ensure that the experiments isolate the effects of changing coastlines and avoids results being influenced by anomalously warm, cold, wet or dry years or periods. An extra year was prepended to the beginning of each WRF run period as model-spin up time. That year was not included in the analyses. The following options were used for WRF model physics: Single moment 6-class scheme for microphysics (Hong and Lim, 2006), CAM scheme for longwave and shortwave radiation (Collins et al., 2004), Unified Noah Model for the land surface (Tewari et al., 2004), ETA similarity scheme for the surface layer (Janjic, 2002), Yonsei University Scheme for planetary boundary layer (Hong et al., 2006), and Kain–Fritsch scheme for cumulus parameterization (Kain, 2004).

The two WRF simulations performed at 70 ka, *CTRL* and *ExpLand*, are shown in Table 1. The only difference between these two simulations is their land-sea mask (explained in more detail in the next subsection). The WRF source code was modified accordingly in order for the model to use correct radiation values, as done in Yoo and Galewsky (2016). High resolution sea surface temperature (SST) input fields for WRF simulations were created using the *anomaly method* described by Haywood et al. (2010) and Zhang and Yan (2012). This approach ensures an improved representation of SSTs in the regional model, compared to using the raw SST output from the global model directly. It thus results in a more realistic simulation of near surface variables and precipitation, especially over coastal areas. In this study, the method was implemented by adding monthly long-term differences between modern SSTs and NorESM pre-industrial SSTs (i.e., the anomaly) to the monthly, raw SST fields of NorESM at 70 ka. Long term monthly mean SSTs were obtained from the ERA5 reanalysis (Hersbach et al., 2020), averaged over the 1981–2000 period at each month. Raw NorESM SST fields were first regridded into ERA5 grid (0.25° resolution), using the ESMF regrid routine of the NCAR Command Language (NCL).

Table 1
WRF simulations performed at 70 ka.

GCM name and version	RCM (WRF) Simulation at 70 ka	Sea Level Difference wrt Present
NorESM-1F	Control (*CTRL*)	0 m
NorESM-1F	Exposed Land (*ExpLand*)	−80 m

3.3. Coastline changes

To simulate the effects of glacial variation on coastal land extent, the WRF land-sea mask was modified for the *ExpLand* simulation, assuming a sea level drop of 80 m at 70 ka with respect to present day (Fig. 1b, *ExpLand* stands for exposed land). −80 m is the maximum likelihood estimate of relative sea level at 70 ka as reconstructed by Grant et al. (2012), with the lower and upper bounds of the 95% confidence interval at ~ 70 and 90 m, respectively (Supp. Fig.). This record correlates well with the sea level index points determined by Cawthra et al. (2018) for the southern continental shelf of South Africa, in addition to having lower age uncertainties and a higher temporal resolution compared to other available sea level reconstructions (Spratt and Lisiecki, 2016). For the *ExpLand* simulation, each original land grid cell in the model topography was lifted by 80 m. Newly exposed cells were determined using ETOPO1 bathymetry data (NOAA National Geophysical Data Center, 2009). Vegetation type of the exposed cells were set to the dominant type in the neighboring cells. Present day land extent was used in the control (CTRL) simulation. Present day vegetation cover was used in both simulations, with the exception of urban and crop cells, which were replaced with the dominant vegetation type from the neighboring cells.

4. Results and discussion

Sensitivity of the southern African climate to changes in sea level and associated land extent is assessed by comparing output from the two RCM simulations, *ExpLand* and *CTRL*. Both simulations were driven by boundary conditions provided by the same GCM output at 70 ka. They are identical in all respects, except for their land-sea masks (see Section 3.3 and Fig. 1).

Differences in the 30-year averages of *ExpLand* and *CTRL* simulations were analyzed. There is no indication of significant large-scale *circulation* differences between the two (not shown). This is as expected given the experimental design, but is nonetheless important as it confirms that internal variability within the RCM domain does not have a strong impact. Large differences in temperature and precipitation occur only over and around coastal regions, where areas previously covered by ocean (*CTRL*) are exposed due to the sea-level drop (*ExpLand*). These differences are a direct response to the shifting coastline, which puts many present-day coastal sites far from the ocean, making them relatively more continental.

4.1. Surface air temperature

Mean temperatures inland are slightly lower in the *ExpLand* simulation compared to *CTRL* (Fig. 2), owing to the lower sea level and therefore an overall higher topography. Differences in daily maximum and minimum temperatures, along with surface wind anomalies, are shown for the southern Cape and adjacent regions in Fig. 3. This figure is a clear demonstration of the fact that, as the shoreline retreats, areas that were once coastal and are now inland switch to a more continental climate, with cooler nights and warmer days. Where the amplitude of nighttime cooling is greater than daytime warming, there is a decrease in mean temperatures compared to the *CTRL* simulation (Fig. 2). Likewise, stronger daytime warming (compared to nighttime cooling) leads to an increase in the mean temperature. Austral winter (JJA) nighttime cooling is especially pronounced over the Palaeo-Agulhas Plain, with a mean decrease of 2−5 °C compared to the *CTRL* simulation (Fig. 3). While daytime warming in austral winter is modest (~2 °C), it is much larger in austral summer (DJF), with increases of over 5 °C around western Cape, and 3−4 °C in the south in the *ExpLand* simulation. It is worth noting that the magnitude of these temperature changes are of the same order as the estimated differences between Last Glacial Maximum and pre-industrial by global models (Stone, 2014). Moreover, changes during austral summer, especially the daytime temperature increases, extend well inland, where the climate was already continental before the coastline shift (Fig. 3, right panel). This appears to be the result of the surface winds having an increased northerly component in the *ExpLand* run in summer, inducing a land breeze mechanism that should further lessen the maritime influence. This also highlights the importance of local wind changes in modulating coastal climates, even when there is no large-scale signal.

Overall, the coastline shift results in a significant increase of the diurnal temperature range. This also leads to lower winter and higher summer mean temperatures, as nighttime cooling and daytime warming/reduced sea-breeze dominate during winter and summer, respectively. These changes are shown in more detail in Fig. 4 for the WRF grid cell that is closest to Blombos Cave. In all months (except March), the lower quartile of daily minimum temperatures after the coastline shift (*ExpLand*) is entirely within the lower 1st percentile of the same variable before the shift (*CTRL*). In June and July, ~40% of daily minimums in the ExpLand simulation would be outliers (i.e. lower 1st percentile) in the *CTRL*. This means that, owing only to coastline shift, the probability of having an exceptionally *cold* night around Blombos Cave (by the control simulation's marine climate standard), increases from 1% to 25−30% in all months (except March), and to ~ 40% in June and July. The shift in summer maximum temperatures is even more remarkable owing to the northerly component of the surface wind difference. More than 50% of all *ExpLand* daily maximums from November to February lie beyond the upper 1st percentile in the *CTRL* simulation (Fig. 4); while the same metric is greater than 75% from December to January. In other words, the probability of getting a 'one in a hundred' summer heat event increases 50- to 75-fold with the coastline shift.

These changes in the temperature regime were detected in the analysis of extremes (Fig. 5) and selected climate indices (Figs. 8 and 9) as well. Due to the coastline shift, monthly absolute maximum (minimum) temperatures shift to higher (lower) values, putting the vast majority of the monthly extremes in the *ExpLand* simulation outside the ranges of extremes in the *CTRL* simulation for the Blombos Cave locality (Fig. 5). During the warmer half of the year (November to March), *all* the warm monthly temperature extremes simulated in *ExpLand* are warmer than those in *CTRL* (Fig. 5), further highlighting the local effects related to changes in the sea breeze during summer (Fig. 3). The warmest extreme for Blombos Cave locality in *ExpLand* is ~15 °C warmer than that in *CTRL* (Fig. 5). Likewise, the mean annual number of days with a T_{max} greater than 25 °C (summer days) or a T_{min} less than 5 °C at Blombos Cave jumps from almost none (0.1 and 0.6, respectively) in *CTRL* to 40.6 and 30.1 in *ExpLand*, respectively (Fig. 9). These more continental temperatures in the *ExpLand* simulation are a regionally consistent climatic feature of the areas where the coastline retreats (Fig. 8). As evident from the more numerous summer days (Fig. 8), daytime warming over previously coastal localities is especially strong. This is in contrast with inland locations where the same metric shows a slight decrease due to the 80 m elevation increase in the *ExpLand* simulation.

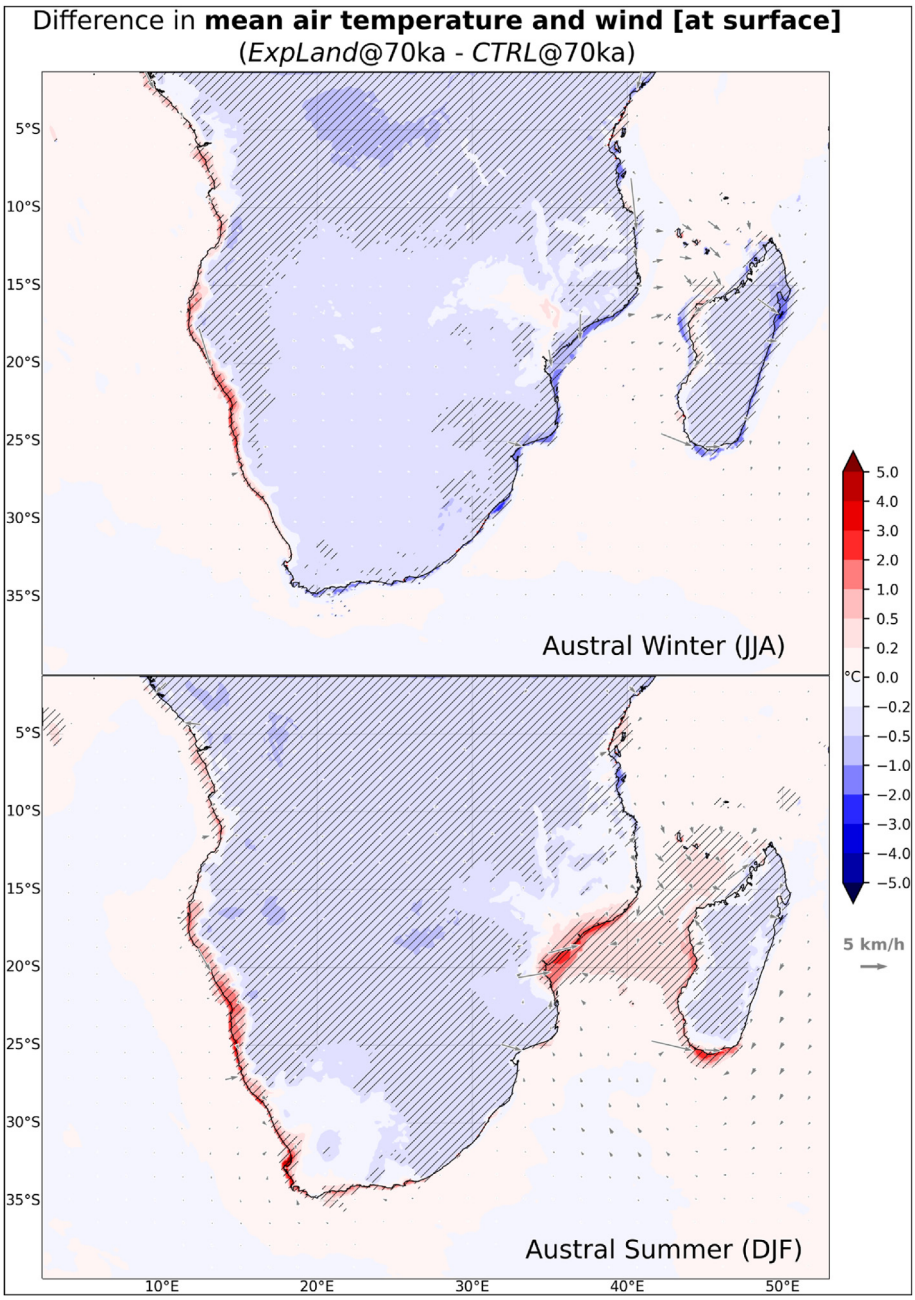

Fig. 2. 30-year difference in mean surface air temperature (blue/red shadings) and surface winds (grey vectors) between *ExpLand* and *CTRL* simulations at 70 ka. Top: Austral winter (JJA). Bottom: Austral summer (DJF). Statistically significant differences in temperature (*t*-test, 95% confidence level) are hatched. Present coastline is plotted. (For interpretation of the references to colour in this figure legend, the reader is referred to the Web version of this article.)

4.2. Precipitation

Long-term mean *ExpLand* - *CTRL* differences in precipitation indicate local reductions of 5–40% along the southern and western Cape coasts and over exposed land as the coastline shifts seaward (Fig. 6, left panel). Lower amounts of precipitation in the *ExpLand* simulation are likely due to increased frictional drag on low level winds caused by the extra land mass near coastal areas, which prevents marine moisture from penetrating further inland. This is evident, for instance around Blombos Cave, from the easterly and northwesterly wind difference vectors in austral winter and summer, respectively (Fig. 6), indicating a slowdown of moisture-laden low-level flow from the ocean. Also, around Blombos, there is a relatively larger area of reduced precipitation in austral summer compared to winter, extending towards inland (Fig. 6). This owes to the weaker southerly component of surface winds in summer in

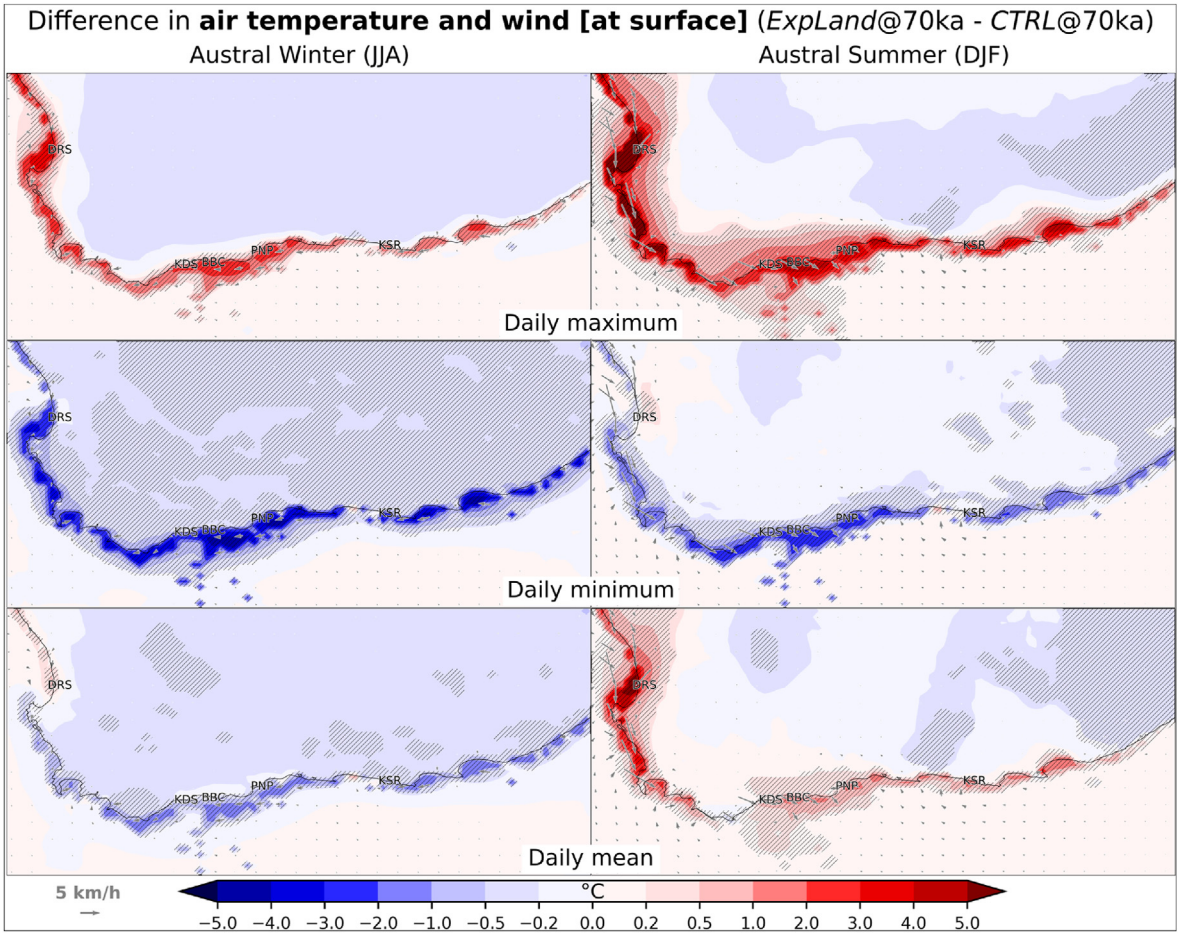

Fig. 3. 30-year mean difference in daily maximum, minimum and mean surface air temperatures (blue/red shadings), and surface winds (grey vectors); between *ExpLand* and *CTRL* simulations at 70 ka, for austral winter (JJA, left) and austral summer (DJF, right). Areas of statistically significant temperature differences (*t*-test, 95% confidence level) are hatched. All visible wind anomaly vectors denote statistically significant speed differences either of the *u* or the *v*-wind. Present coastline is plotted. Locations of the archaeological sites in Fig. 1b are also marked. (For interpretation of the references to colour in this figure legend, the reader is referred to the Web version of this article.)

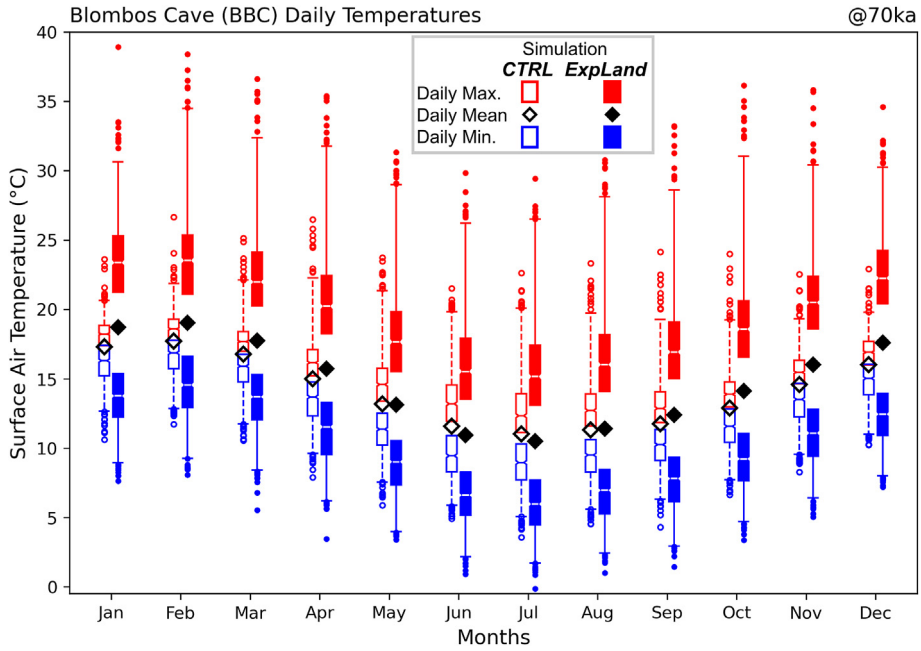

Fig. 4. Daily maximum, minimum and mean surface air temperatures at around Blombos Cave locality through the 30-year simulation period of WRF model at 70 ka, for both *ExpLand* and *CTRL* simulations. Only the long-term monthly averages are shown for daily means (black diamonds), whereas daily extremes are summarized as box-and-whisker plots. End of whiskers denote the 99th (1st) percentile for daily maximum (minimum) temperatures at each month. For the sake of readability, lower (upper) whiskers of daily maximums (minimums) are not shown.

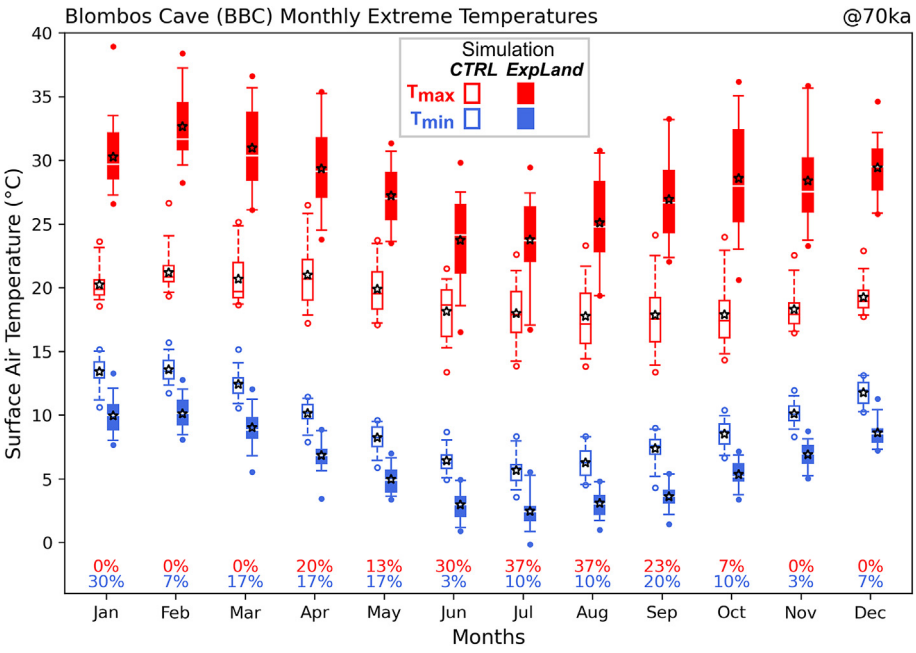

Fig. 5. Monthly absolute maximum and minimum surface air temperatures (box-and-whisker plots) at around Blombos Cave in each of the 30 years at 70 ka, for both *ExpLand* and *CTRL* simulations. End of whiskers denote upper 99th and lower 1st percentiles at each month. Stars show long-term means of monthly extremes. Percentage values at the bottom of the plot indicate the portion of the extremes in the *ExpLand* simulation that are within the range of extremes in *CTRL* simulation, at each month.

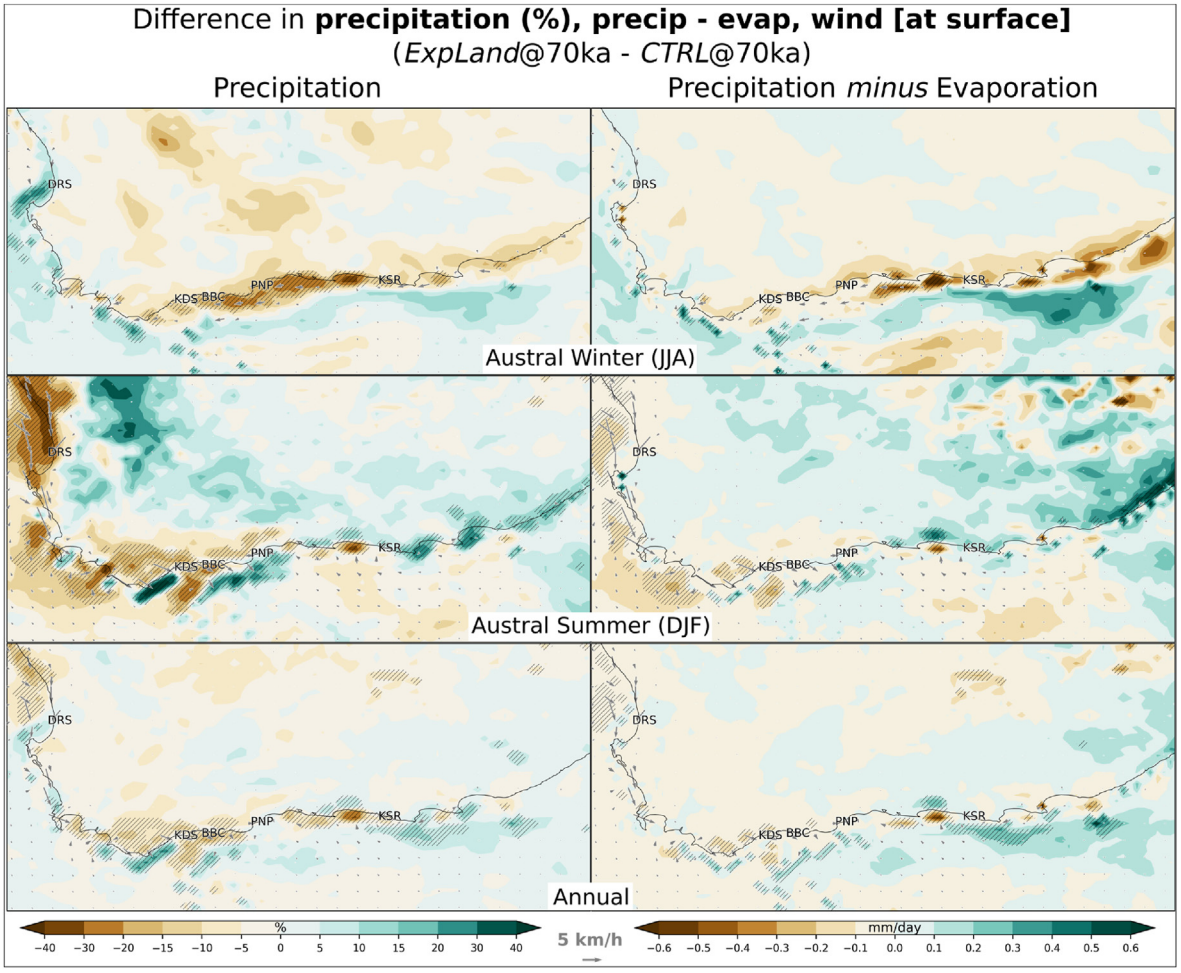

Fig. 6. 30-year mean difference in precipitation amounts (brown/green shadings, left panel), precipitation minus evaporation values (brown/green shadings, right panel) and surface winds (overlain grey vectors), between *ExpLand* and *CTRL* simulations at 70 ka. Areas of statistically significant changes (*t*-test, 95% confidence level) are hatched. Precipitation *minus* evaporation values on the exposed land areas are masked. All visible wind anomaly vectors denote statistically significant speed differences either of the *u* or the *v*-wind. Present coastline is plotted. Locations of the five archaeological sites in Fig. 1b are also marked. (For interpretation of the references to colour in this figure legend, the reader is referred to the Web version of this article.)

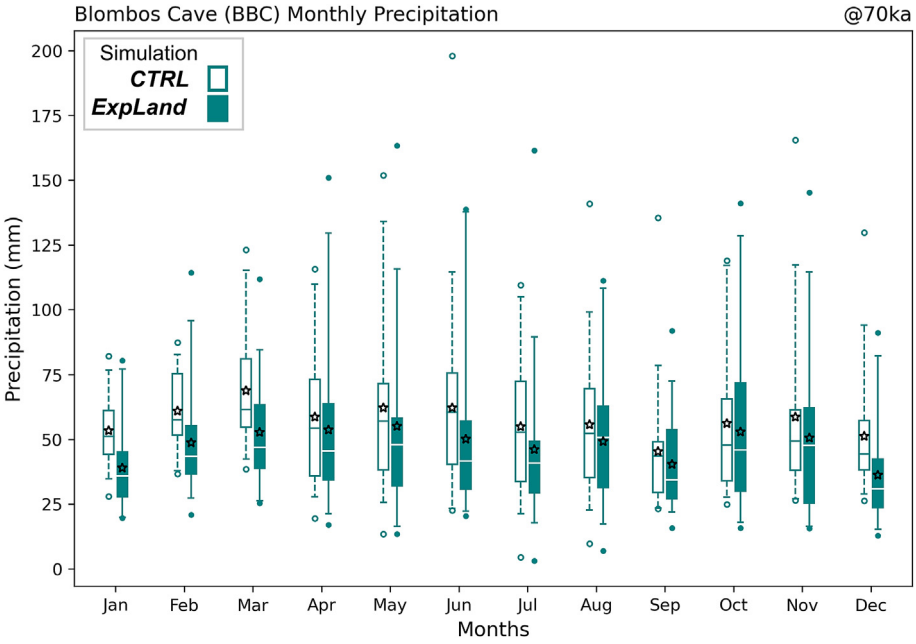

Fig. 7. Monthly precipitation amounts (box-and-whisker plots) at around Blombos Cave in each of the 30 years at 70 ka, for both *ExpLand* and *CTRL* simulations. End of whiskers denote upper 99th and lower 1st percentiles for monthly precipitation at each month. Stars show long-term monthly means.

ExpLand (note the northerly component of the wind difference vector in Fig. 6), which was not simulated for winter. Accordingly, the reduction in summer rainfall (25%) around Blombos Cave is greater than in winter (16%) and other seasons. Nevertheless, there is less rainfall around the Cave in the *ExpLand* simulation at every month of the year (Fig. 7), corresponding to a statistically significant 17% reduction in the annual precipitation amount with respect to the *CTRL* simulation.

Contributing to the decreasing precipitation amounts, there are significantly fewer rainy days in the southern and western Cape coasts in response to the coastline shift (Fig. 8). The largest changes occur near the southern coast, with the mean annual number of rainy days (daily precipitation $\geq$1 mm) for the Blombos Cave area falling from 152 to 121 (Fig. 9). Statistically significant increases were simulated for the maximum length of dry spell within a year too (Fig. 8), though these changes are not as strong as the decrease in the number of rainy days, especially over the southern Cape coast. The mean length of longest dry spell rises from 13.9 to 16.1 days for the Blombos Cave area (Fig. 9). There is no significant change in the 5-day maximum precipitation amounts.

The drying implied by the precipitation decline is not entirely corroborated by the changes in precipitation minus evaporation (P-E) from *CTRL* to *ExpLand* (Fig. 6, right panel). P-E values decrease less than precipitation does, since surface evaporation drops in tandem with rainfall (not shown). Increases in mean temperatures from *CTRL* to *ExpLand* are confined to austral summer months and are smaller compared to the changes in daily extremes (Fig. 4), so this might play a role in keeping P-E changes smaller, by suppressing further evaporation in the *ExpLand* simulation. Note also that the changes in P-E over the exposed land areas in the right panel of Fig. 6 are masked, as evaporation from sea and land are not comparable.

5. Summary and conclusions

In this study we employed a targeted modelling approach to demonstrate the influence that coastline shifts had on local climates in the southern Cape of South Africa around 70 ka . Our results indicate substantial *local-to-regional* changes, arising solely in response to land extent variations. The overall effect of the coastline retreat on the previously coastal localities is a shift to more continental temperature regimes that feature warmer days and summers, also cooler nights and winters. Additionally, we found significant year-round reductions in rainfall amounts and in the number of rainy days. All these changes are especially pronounced along the southern coast, where the areal extent of the exposed land due to seaward coastline shift is the largest along the Cape coast. Our regional climate model simulations allow for more details to emerge, demonstrating a seasonally and locally varying response in both temperature and precipitation to coastline retreat. Specifically, changes are stronger and spread further inland in summer compared to winter near Blombos Cave, with a large increase in daytime temperatures and somewhat more pronounced precipitation reduction. These are attributable to seasonally distinct modifications in the local atmospheric circulation and in the sea breeze mechanism, which arise solely because of the exposed land.

While it is beyond the scope of the present work to make causal links between climate and early human behaviour, the results here do provide some support for a link between coastline position, local climate and human behaviour. If ancient humans chose to live close to the shoreline because the sea, besides providing food, also moderated temperatures and enhanced rainfall, then at least *some* of those coastal people may have chased the shoreline as it moved away. This way, they could have reached the environment and climate they were used to and preferred. The increases in the simulated interseasonal and diurnal range of temperatures when

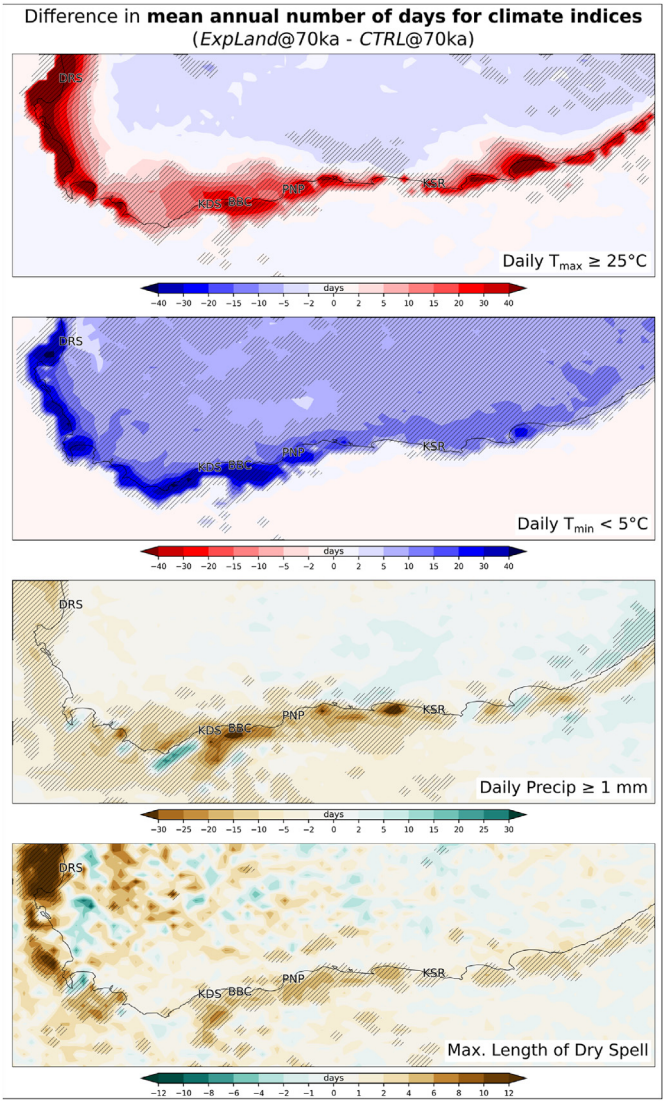

Fig. 8. 30-year mean difference in four selected climate indices, between *ExpLand* and *CTRL* simulations at 70 ka. Areas of statistically significant changes (*t*-test, 95% confidence level) are hatched. Present coastline is plotted. Locations of the five archaeological sites in Fig. 1b are also marked.

the coastline moved further away as sea levels dropped (Figs. 3 and 4), as well as the reduction in precipitation (Figs. 6 and 7), suggests that the marine-to-continental climate transition might have triggered this behaviour. These shoreline-following groups of ancient people could have found more space to explore across the expanded coastal plain, which is known to have provided numerous coastal routes for migration and resource acquisition (e.g., Armitage et al., 2011). Recent findings from Blombos Cave (Haaland et al., 2020) support this view as they indicate increased mobility of hunter gatherers during times of relatively distant seashore, with shorter but more frequent visits to the cave. We speculate that the local increase in the continentality of climate due to the moving shoreline, which are quantified for the first time in our study, may have been a factor in determining mobility patterns of early humans.

There are still many additional questions to consider. One relates to the relative role of the coastline shift compared to that of orbital

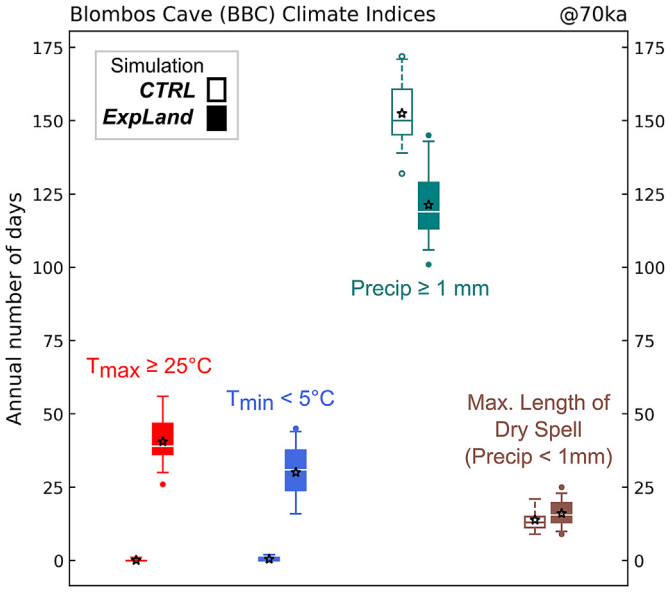

Fig. 9. Selected four climate indices (box-and-whisker plots) around Blombos Cave in each of the 30 years at 70 ka, for both *ExpLand* and *CTRL* simulations. End of whiskers denote upper 99th and lower 1st percentiles. Stars show long-term means.

and greenhouse gas forcing. Although our results suggest that the marine-to-continental climate transition in southern Africa due to the moving coastline might have been large enough by itself to influence early humans, we do not yet know whether these changes would be amplified or dampened in the presence of other climate forcings. Research on this question is ongoing and will be the subject of a follow-up manuscript, which will investigate the climatic evolution of the region using both models and proxy data from Blombos Cave. Other questions such as, just how much these environmental changes mattered for the development of technological and symbolic culture are outstanding. Despite good agreement between the physical climate models and the evidence of human activity in Blombos Cave, even with future evidence from paleoproxies; any causal link between climate and human development is necessarily speculative. An intriguing future direction would be to integrate regional scale environmental information with human agency using agent-based models to better explore how early humans interacted with their local environment. While these models have been used extensively to explore large-scale (e.g. out of Africa) migration and dispersion, they have yet to be applied in local to regional contexts such as that of southern Africa.

Declaration of competing interest

The authors declare that they have no known competing financial interests or personal relationships that could have appeared to influence the work reported in this paper.

Data availability

Data will be made available on request.

Acknowledgments

We thank Priscilla Mooney and Deniz Bozkurt for their technical support throughout WRF model set-up and simulations, John

Galewsky for providing his modified WRF source code that implements the use of paleo-orbital parameters, and Jimwoong Yoo for his explanations of the aforementioned code. We also thank Francesco Pausata for his constructive critique of the manuscript and helpful suggestions. High performance computing and storage services were provided by Norwegian Research Infrastructure Services (NRIS) through Notur/NorStore projects NN9486K and NS9486. This work was partly supported by the Research Council of Norway, through its Centres of Excellence funding scheme, SFF Centre for Early Sapiens Behaviour (SapienCE), project number 262618.

Appendix A. Supplementary data

Supplementary data to this article can be found online at https://doi.org/10.1016/j.quascirev.2022.107893.

References

Armitage, Simon J, Jasim, Sabah A, Marks, Anthony E, Parker, Adrian G, Usik, Vitali I, Uerpmann, Hans-Peter, 2011. The southern route "out of Africa": evidence for an early expansion of modern humans into Arabia. Science. https://doi.org/10.1126/science.1199113.

Berger, A., Loutre, M.F., 1991. Insolation values for the climate of the last 10 million years. Quat. Sci. Rev. 10, 297–317.

Braun, K., Bar-Matthews, M., Matthews, A., Ayalon, A., Cowling, R., Karkanas, P., Marean, C., 2019. Late Pleistocene records of speleothem stable isotopic compositions from Pinnacle Point on the South African south coast. Quat. Res. 91 (1), 265–288. https://doi.org/10.1017/qua.2018.61.

Caley, T., Extier, T., Collins, J.A., Schefuss, E., Dupont, L.M., Malaizé, B., Rossignol, L., Souron, A., McClymont, E.L., Jiménez-Espejo, F.J., García-Comas, C., Eynaud, F., Martinez, P., Roche, D.M., Jorry, S.J., Charlier, K., Wary, M., Gourves, P., Billy, I., Giraudeau, J., 2018. A two-million-year-long hydroclimatic context for hominin evolution in southeastern Africa. Nature 560, 76–79.

Cawthra, H.C., Jacobs, Z., Compton, J.S., Fisher, E.C., Karkanas, P., Marean, C.W., 2018. Depositional and sea-level history from MIS 6 (Termination II) to MIS 3 on the southern continental shelf of South Africa. Quat. Sci. Rev. 181, 156–172. https://doi.org/10.1016/j.quascirev.2017.12.002. ISSN 0277-3791.

Cole, M.J., Bailey, R.M., Cullis, J.D.S., New, M.G., 2018. Spatial inequality in water access and water use in South Africa. Water Pol. 20 (1), 37–52. https://doi.org/10.2166/wp.2017.111, 1 February 2018.

Collins, W., Rasch, P., Boville, B., Hack, J., Mccaa, J., Williamson, D., Kiehl, J., 2004. Description of the NCAR Community Atmosphere Model (CAM 3.0). NCAR Technical Note. TN-464+STR.

Crameri, F., 2018. Scientific Colour Maps. Zenodo. https://doi.org/10.5281/zenodo.1243862.

Eichler, T.P., Gottschalck, J., 2013. A comparison of southern hemisphere cyclone track climatology and interannual variability in coarse-gridded reanalysis datasets. Adv. Meteorol. https://doi.org/10.1155/2013/891260. Article ID 891260, 16.

Engelbrecht, F.A., Marean, C.W., Cowling, R.M., Engelbrecht, C.J., Neumann, F.H., Scott, L., Nkoana, R., O'Neal, D., Fisher, E., Shook, E., Franklin, J., Thatcher, M., McGregor, J.L., Van der Merwe, J., Dedekind, Z., Difford, M., 2019. Downscaling last glacial maximum climate over southern africa. *Quat. Sci. Rev.* Issue 226, 105879. https://doi.org/10.1016/j.quascirev.2019.105879.

Eriksson, A., Betti, L., Friend, A.D., Lycett, S.J., Singarayer, J.S., von Cramon-Taubadel, N., Valdes, P.J., Balloux, F., Manica, A., 2012. Late Pleistocene climate change and the global expansion of anatomically modern humans. Proc. Natl. Acad. Sci. USA 109 (40), 16089–16094. https://doi.org/10.1073/pnas.1209494109. Epub 2012 Sep 17. PMID: 22988099; PMCID: PMC3479575.

Fick, S.E., Hijmans, R.J., 2017. WorldClim 2: new 1-km spatial resolution climate surfaces for global land areas. Int. J. Climatol. 37, 4302–4315. https://doi.org/10.1002/joc.5086.

Fisher, E., Cawthra, H., Esteban, I., Jerardino, A., Neumann, F., Oertle, A., Pargeter, J., Saktura, R.B., Szabo, K., Winkler, S., Zohar, I., 2020. Coastal occupation and foraging during the last glacial maximum and early Holocene at Waterfall Bluff, eastern Pondoland, South Africa. Quat. Res. 97, 1–41. https://doi.org/10.1017/qua.2020.26.

Grant, K., Rohling, E., Bar-Matthews, M., Ayalon, A., Medina-Elizalde, M., Bronk Ramsey, C., Satow, C., Roberts, A.P., 2012. Rapid coupling between ice volume and polar temperature over the past 150,000 years. Nature 491, 744–747. https://doi.org/10.1038/nature11593.

Guo, C., Bentsen, M., Bethke, I., Ilicak, M., Tjiputra, J., Toniazzo, T., Schwinger, J., Otterå, O.H., 2019. Description and evaluation of NorESM1-F: a fast version of the Norwegian Earth system model (NorESM). Geosci. Model Dev. (GMD) 12, 343–362. https://doi.org/10.5194/gmd-12-343-2019.

Haaland, M., Miller, C., Unhammer, O., Reynard, J., Van Niekerk, K., Ligouis, B., Mentzer, S.M., Henshilwood, C.S., 2020. Geoarchaeological investigation of occupation deposits in Blombos Cave in South Africa indicate changes in site use and settlement dynamics in the southern Cape during MIS 5b-4. Quat. Res. 1–54. https://doi.org/10.1017/qua.2020.75.

Haywood, A.M., Dowsett, H.J., Otto-Bliesner, B., Chandler, M.A., Dolan, A.M., Hill, D.J., Lunt, D.J., Robinson, M.M., Rosenbloom, N., Salzmann, U., Sohl, L.E., 2010. Pliocene model intercomparison project (PlioMIP): experimental design and boundary conditions (experiment 1). Geosci. Model Dev. (GMD) 3, 227–242. https://doi.org/10.5194/gmd-3-227-2010.

Henshilwood, C.S., 2012. Late Pleistocene techno-traditions in southern africa: a review of the still bay and howiesons poort, c. 75–59 ka. J. World Prehist 25, 205–237. https://doi.org/10.1007/s10963-012-9060-3.

Henshilwood, C.S., van Niekerk, K.L., Wurz, S., Delagnes, A., Armitage, S.J., Rifkin, R.F., Douze, K., Keene, P., Haaland, M.M., Reynard, J., Discamps, E., Mienies, S.S., 2014. Klipdrift shelter, southern Cape, South Africa: preliminary report on the howiesons poort layers. J. Archaeol. Sci. 45, 284–303. https://doi.org/10.1016/j.jas.2014.01.033.

Hersbach, H., Bell, B., Berrisford, P., et al., 2020. The ERA5 global reanalysis. Q. J. R. Meteorol. Soc. 146, 1999–2049. https://doi.org/10.1002/qj.3803.

Hong, S.Y., Lim, J.O.J., 2006. The WRF single–moment 6–class microphysics scheme (WSM6). J. Korean Meteor. Soc. 42, 129–151.

Hong, S.Y., Yign, N., Dudhia, J., 2006. A new vertical diffusion package with an explicit treatment of entrainment processes. Mon. Weather Rev. 134, 2318–2341.

Janjic, Z.I., 2002. Nonsingular implementation of the mellor-yamada level 2.5 scheme in the NCEP meso model. NCEP Off. Note No 437, 61.

Kain, J.S., 2004. The Kain–Fritsch convective parameterization: an update. J. Appl. Meteorol. 43, 170–181.

Lambeck, K., Chappell, J., 2001. Sea level change through the last glacial cycle. Science 292, 679–686.

Lesnek, A.J., Briner, J.P., Lindqvist, C., Baichtal, J.F., Heaton, T.H., 2018. Deglaciation of the Pacific coastal corridor directly preceded the human colonization of the Americas. Sci. Adv. 4 (5), eaar5040. https://doi.org/10.1126/sciadv.aar5040.

Levitus, S., Boyer, T.P., 1994. World Ocean Atlas Volume 4: Temperature, NOAA Atlas NESDIS 4. US Government Printing Office, Washington, DC, p. 117.

Marean, C., Bar-Matthews, M., Bernatchez, J., et al., 2007. Early human use of marine resources and pigment in South Africa during the Middle Pleistocene. Nature 449, 905–908. https://doi.org/10.1038/nature06204.

Marean, C.W., Cowling, R.M., Franklin, J., 2020. The Palaeo-Agulhas Plain: temporal and spatial variation in an extraordinary extinct ecosystem of the Pleistocene of the Cape floristic region. Quat. Sci. Rev. 235. https://doi.org/10.1016/j.quascirev.2019.106161.

Martínez-Botí, M., Foster, G., Chalk, T., Rohling, E.J., Sexton, P.F., Lunt, D.J., Pancost, R.D., Badger, M.P.S., Schmidt, D.N., 2015. Plio-Pleistocene climate sensitivity evaluated using high-resolution CO2 records. Nature 518, 49–54. https://doi.org/10.1038/nature14145.

NOAA National Geophysical Data Center, 2009. ETOPO1 1 Arc-Minute Global Relief Model. NOAA National Centers for Environmental Information. (Accessed 15 September 2019).

Partridge, T.C., de Menocal, P.B., Lorentz, S.A., Paiker, M.J., Vogel, J.C., 1997. Orbital forcing of climate over South Africa: a 200,000-year rainfall record from the pretoria saltpan. Quat. Sci. Rev. 16 (10), 1125–1133. https://doi.org/10.1016/S0277-3791(97)00005-X. ISSN 0277-3791.

Powers, J.G., Klemp, J.B., Skamarock, W.C., Davis, C.A., Dudhia, J., Gill, D.O., Coen, J.L., Gochis, D.J., Ahmadov, R., Peckham, S.E., Grell, G.A., Michalakes, J., Trahan, S., Benjamin, S.G., Alexander, C.R., Dimego, G.J., Wang, W., Schwartz, C.S., Romine, G.S., Liu, Z., Snyder, C., Chen, F., Barlage, M.J., Yu, W., Duda, M.G., 2017. The weather research and forecasting model: overview, system efforts, and future directions. Bull. Am. Meteorol. Soc. 98 (8), 1717–1737.

Rae, J.W.B., Gray, W.R., Wills, R.C.J., Eisenman, I., Fitzhugh, B., Fotheringham, M., Littley, E.F.M., Rafter, P.A., Rees-Owen, R., Ridgwell, A., Taylor, B., Burke, A., 2020. Enhanced overturning circulation in the glacial North Pacific caused warming, nutrient limitation, and lower atmospheric CO_2. Sci. Adv., eabd1654

Raia, P., Mondanaro, A., Melchionna, M., Di Febbraro, M., Diniz-Filho, J.A.F., Rangel, T.F., Holden, P.B., Carotenuto, F., Edwards, N.R., Lima-Ribeiro, M.S., Profico, A., Maiorano, L., Castiglione, S., Serio, C., Rook, L., 2020. Past extinctions of Homo species coincided with increased vulnerability to climatic change. One Earth 3 (4), 480–490. https://doi.org/10.1016/j.oneear.2020.09.007.

Rohling, E.J., Foster, G.L., Grant, K.M., Marino, G., Roberts, A.P., Tamisiea, M.E., Williams, F., 2014. Sea-level and deep-sea-temperature variability over the past 5.3 million years. Nature 508, 477–482.

Sime, L., Kohfeld, K.E., Le Quéré, C., Wolff, E.W., de Boer, A.M., Graham, R.M., Bopp, L., 2013. Southern Hemisphere westerly wind changes during the Last Glacial Maximum: model-data comparison. Quat. Sci. Rev. 64, 104–120. https://doi.org/10.1016/j.quascirev.2012.12.008. ISSN 0277-3791.

Simon, M., Ziegler, M., Bosmans, J., Barker, S., Reason, C.J.C., Hall, I.R., 2015. Eastern South African hydroclimate over the past 270,000 years. Nat. Sci. Rep. 5, 18153. https://doi.org/10.1038/srep18153.

Skamarock, W.C., Klemp, J.B., Dudhia, J., Gill, D.O., Liu, Z., Berner, J., Huang, X., 2019. A Description of the Advanced Research WRF Model Version 4 (No. NCAR/TN-556+STR). https://doi.org/10.5065/1dfh-6p97.

Spratt, R.M., Lisiecki, L.E., 2016. A Late Pleistocene sea level stack. Clim. Past 12, 1079–1092. https://doi.org/10.5194/cp-12-1079-2016.
Stone, A.E.C., 2014. Last Glacial Maximum conditions in southern Africa: are we any closer to understanding the climate of this time period? Prog. Phys. Geogr.: Earth Environ. 38 (5), 519–542. https://doi.org/10.1177/0309133314528943.
Strobel, P., Bliedtner, M., Carr, A.S., Frenzel, P., Klaes, B., Salazar, G., Struck, J., Szidat, S., Zech, R., Haberzettl, T., 2020. Holocene Sea Level and Environmental Change at the Southern Cape – an 8.5 Kyr Multi-Proxy Paleoclimate Record from Lake Voëlvlei, South Africa Climate of the Past Discussions, pp. 1–37.
Tewari, M., Chen, F., Wang, W., Dudhia, J., LeMone, M.A., Mitchell, K., Ek, M., Gayno, G., Wegiel, J., Cuenca, R.H., 2004. Implementation and verification of the unified NOAH land surface model in the WRF model. In: 20th Conference on Weather Analysis and Forecasting/16th Conference on Numerical Weather Prediction, pp. 11–15.
Texier, P.J., Porraz, G., Parkington, J., Rigaud, J.P., Poggenpoel, C., Tribolo, C., 2013. The context, form and significance of the MSA engraved ostrich eggshell collection from Diepkloof Rock Shelter, Western Cape, South Africa. J. Archaeol. Sci. 40-9, 3412–3431. https://doi.org/10.1016/j.jas.2013.02.021. ISSN 0305-4403.
Timmermann, A., 2020. Quantifying the potential causes of Neanderthal extinction: abrupt climate change versus competition and interbreeding. Quat. Sci. Rev. 238, 1–33.
Timmermann, A., Friedrich, T., 2016. Late Pleistocene climate drivers of early human migration. Nature 538, 92–95.
Wurz, S., 2002. Variability in the middle stone age lithic sequence, 115,000 - 60,000 years ago at Klasies River, South Africa. J. Archaeol. Sci. 29, 1001–1015.
Yoo, J., Galewsky, J., 2016. Dynamical downscaling of the western North Pacific from CCSM4 simulations during the last glacial maximum and late 20th century using the WRF model: model configuration and validation. Clim. Past Discuss 1–33.
Zhang, Z., Yan, Q., 2012. Pre-industrial and mid-Pliocene simulations with NorESM-L: AGCM simulations. Geosci. Model Dev. (GMD) 5, 1033–1043. https://doi.org/10.5194/gmd-5-1033-2012.